11. J. J. Hickman, D. Ofer, P. E. Laibinis, G. M. Whitesides, M. S. Wrighton, *ibid.*, **113**, 1128 (1991).
12. The microelectrode arrays consist of eight wires (~2 μm wide by ~50 μm long by ~0.1 μm thick) separated from each other by ~1.4 μm on a flat Si_3N_4-coated Si substrate [G. P. Kittlesen, H. S. White, M. S. Wrighton, *J. Am. Chem. Soc.* **106**, 7389 (1984)]. The leads connecting the microelectrodes to macroscopic bonding pads were encapsulated under an additional layer of Si_3N_4. The electrodes were electrochemically plated with an additional layer of fresh Au and cleaned by sonication and then further cleaned in an O_2 plasma for 8 min, after which oxide was reduced by treatment for 2 min in an H_2 plasma. All eight microelectrodes were derivatized and used as one sensor electrode of ~10^3 μm^2 area.
13. Preparation of 2-(8-mercaptooctyl) hydroquinone involved several steps: 1,4-dimethoxy-benzene was deprotonated with *n*-butyllithium and added to excess 1,8-dibromooctane; vacuum distillation afforded 2-(8-bromooctyl)-1,4-dimethoxybenzene; demethylation was accomplished in quantitative yield with BBr_3; the bromide was displaced by thioacetate; and subsequent hydrolysis under acidic conditions yielded the thiol, which was purified by chromatography. Materials were characterized by ^1H NMR spectroscopy. Analysis: calculated (found) for $C_{14}H_{22}O_2S$: C, 66.10 (66.21); H, 8.72 (8.58); and S, 12.60 (12.57).
14. The molecules were self-assembled onto Au surfaces by placement of the Au into ~1 mM solutions of Fc or QH_2 in tetrahydrofuran (THF) or 1:1 ethanol: hexane. Mixtures of Fc and QH_2 were self-assembled onto Au from a 2:1 QH_2:Fc mixture in THF or in 1:1 ethanol:hexane at a total thiol concentration of ~1 mM. All derivatizations were carried out under Ar at 25°C for ~24 hours.
15. R. W. Murray, in *Electroanalytical Chemistry*, A. J. Bard, Ed. (Dekker, New York, 1984), vol. 13, pp. 191–368, and references therein.
16. E. Laviron, *J. Electroanal. Chem.* **146**, 15 (1983); *ibid.* **164**, 213 (1984).
17. A. B. Fischer, thesis, Massachusetts Institute of Technology, Cambridge (1981).
18. V. D. Parker, in *Electroanalytical Chemistry*, A. J. Bard, Ed. (Dekker, New York, 1986), vol. 14, pp. 1–111.
19. We thank the Office of Naval Research and the Defense Advanced Research Projects Agency for partial support of this research. We acknowledge use of XPS and Auger facilities acquired through the joint Harvard/MIT University Research Initiative funded by the Defense Advanced Research Projects Agency.

6 December 1990; accepted 21 February 1991

Three-Dimensional Readout of Flash X-ray Images of Living Sperm in Water by Atomic-Force Microscopy

T. TOMIE,* H. SHIMIZU, T. MAJIMA, M. YAMADA, T. KANAYAMA, H. KONDO, M. YANO, M. ONO

The imaging of living specimens in water by x-ray microscopy can be greatly enhanced with the use of an intense flash x-ray source and sophisticated technologies for reading x-ray images. A subpicosecond x-ray pulse from a laser-produced plasma was used to record the x-ray image of living sea urchin sperm in an x-ray resist. The resist relief was visualized at high resolution by atomic-force microscopy. Internal structure of the sperm head was evident, and the carbon density in a flagellum was estimated from the relief height.

X-RAY MICROSCOPY (XRM) HAS many potential advantages over electron microscopies (EMs) (*1*). The most favored application is the observation of living cells in water with the use of x-rays in the so-called water-window wavelength region (2.32 to 4.37 nm). Although there have been many synchrotron-radiation XRM studies (*2*) with an exposure time longer than a few seconds, flash exposure is essential for high-resolution imaging (*3*). Although a 100-ns x-ray pulse was used in the first experiment of flash XRM of specimen in water (*4*), the maximum exposure time for high-resolution imaging is considered to be shorter than 1 ns, as discussed below. Such a short duration flash x-ray is currently available only from a laser-produced plasma.

Along with the difficulty of obtaining an intense flash x-ray source, the other major problem in flash XRM has been reading the x-ray images. High-resolution flash XRM is possible at present only in contact XRM, in which the x-ray shadow of a specimen is recorded in the closely contacted x-ray resist. The magnification of the image is achieved in the examination stage of the recorded profile. In the examination by EMs, radiation damage by the electron beam of the resist surface or a replica of the resist relief has been a serious problem (*5*). We have used atomic-force microscopy (AFM) (*6*) because the relief on a nonconducting resist surface can be examined directly without coating or making a replica. In microscopy, one wants to observe both thin and thick features in the same image, and the recording material should have a large dynamic range, contrary to the case of lithography, in which an on-off pattern is required. When a dynamic range is large, the contrast of the image is inevitably low. AFM is a good technique for examining low-contrast topography. Moreover, the relief height can be measured with high precision, which allows us to discuss the density of specimens quantitatively. We report the use of AFM in contact XRM in imaging sea urchin sperm.

After a detailed study of the laser-plasma x-ray source (*7*), we succeeded in obtaining one-shot x-ray image of specimens in water by using a low-energy (2-J) laser pulse (*8*) (Fig. 1). The major concern in using a laser-plasma x-ray source was the effect of ultraviolet (UV) emission and debris from the plasma (*9*). We confirmed experimentally that the contribution of UV emission to resist exposure was negligible. Although the 0.1-μm-thick silicon nitride (Si_3N_4) membrane used as an x-ray window was broken after the x-ray exposure, the debris did not reach the resist surface when a specimen in water was imaged. The water between the membrane and the resist protected the resist surface from the debris. The specimen was the sperm of a sea urchin *Anthocidaris crassisspina* in semen solution. The undiluted semen was stored at 4°C. For the observation, the semen was diluted with a one-quarter volume of artificial seawater. A drop of the diluted semen was sandwiched between the Si_3N_4 membrane and a polymethylmethacrylate (PMMA) x-ray resist. The laser plasma was produced by a frequency-doubled glass laser pulse (500 ps, 2 J). The specimen was placed 6 mm from the x-ray source. The x-ray energy density on the resist was 5 to 10 mJ/cm^2. The main contri-

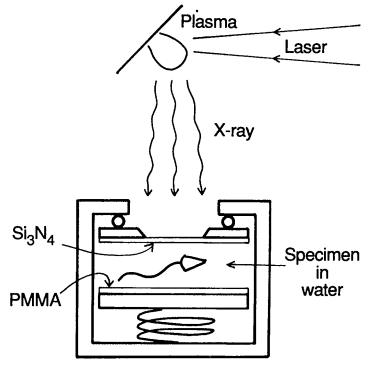

Fig. 1. Experimental configuration. A silicon nitride membrane of 0.1-μm thickness supported on a silicon wafer was used as an x-ray window. The membrane maintained the pressure difference between the vacuum region for the x-ray generation and the atmospheric specimen environment. The x-ray image is recorded in PMMA x-ray resist of 0.5-μm thickness spun on another silicon wafer. The separation between the membrane and the resist was 3 μm and was estimated from the x-ray transmission through water. The minimum separation is limited by the flatness of wafers.

T. Tomie, H. Shimizu, T. Majima, M. Yamada, T. Kanayama, M. Yano, M. Ono, Electrotechnical Laboratory, Tsukuba, Ibaraki, 305 Japan.
H. Kondo, Nikon Corporation, Tsukuba Laboratory, Tsukuba, Ibaraki, 300-26 Japan.

*To whom correspondence should be addressed.

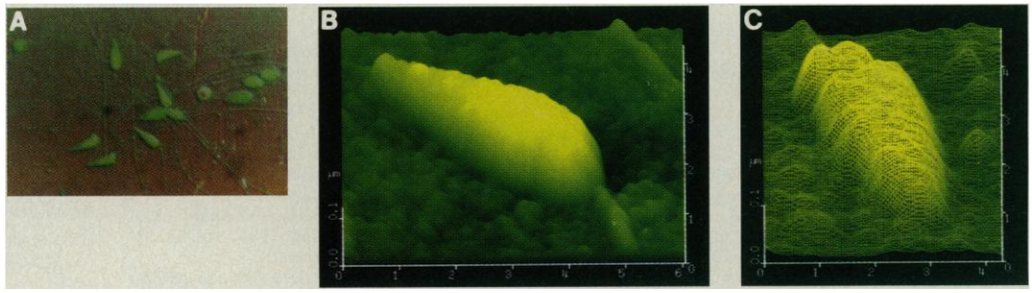

Fig. 2. (**A**) X-ray image of the living sperm of a sea urchin observed in a Normarski optical microscope. The exposed PMMA resist was developed with a 1:1 mixture of methylisobutylketone and isopropanol. The specimen on resist was removed by a sodium hypochlorite solution before development. The image of the 200-μm square x-ray window appeared after 2 min of development, and the development was stopped at 10 min. The developed resist depth was 0.08 μm. From our experimental data on the dissolution rate, the x-ray dose on resist was estimated to be 5 to 10 mJ/cm^2. (**B**) X-ray image of a sperm examined by AFM. The relief height of the head image is 0.075 μm and that of a flagellum is 0.025 μm. The width of the flagellum image is 0.25 μm. (**C**) An AFM image of another sperm head. The AFM display mode is different from that in (B) to show more clearly the structure. Constriction of the image near the neck represents the interface of the nucleus and the mitochondrion. The dent at the neck corresponds to the doughnut shape of the mitochondrion.

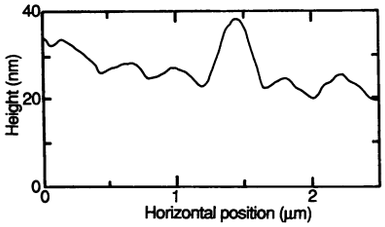

Fig. 3. The width and height of flagella images were modulated with a period of 0.2 to 0.4 μm. The example here shows the relief height along the center of a flagellum image. The modulation could be caused by the flexibility of the flagellum cell membrane.

bution to resist exposure comes from x-rays of 2.4- to 3.0-nm wavelength (*10*).

A photograph of the resist pattern observed in a differential interference optical microscope is shown in Fig. 2A. The x-ray image shows that the sperm have a cone-shaped head 5 μm in length and 1.7 μm in diameter near the neck and a flagellum 40 μm in length. An AFM profile of the sperm head x-ray image is shown in Fig. 2B. The relief height of the head image is 0.075 μm. The flagellum image has a width of 0.25 μm and the height of 0.025 μm.

We note some structure in the sperm head in Fig. 2B. Similar structure could be noticed in all of the sperm heads examined. The structure near the neck is most clearly seen in the sperm shown in Fig. 2C in which the AFM image is displayed in a different output mode. The x-ray image is constricted near the neck, and at the neck the center is dented. The structure of the sperm has been studied through the EM observations of fixed and thin sectioned specimens. Most of the sperm head is occupied by a nucleus, and the mitochondrion is contained near the neck (*11*). The mitochondrion has a doughnut shape around the so-called centriolar fossa. The constriction of the x-ray image corresponds to the interface of the nucleus and the mitochondrion, and the dent corresponds to the doughnut shape of the mitochondrion. These images demonstrate the capability of XRM for observing internal structures of living cells.

As described above, the width of flagellum image is 0.25 μm. From the 0.025-μm height of the flagellum image, the thickness of the actual flagellum is estimated to be equivalent to a 0.15-μm-thick layer of carbon with a density of 1 g/cm^3 (*12*). The carbon density in the flagellum would be 0.6 g/cm^3 if the flagellum has a cylindrical shape, which is in qualitative agreement with the value expected for living cells (*13*). Precise measurement of the relief height by AFM enables us to estimate quantitatively the fraction of elements in specimens. In the flagella images, a modulation in the width and height of a 0.2- to 0.4-μm period is seen. An example is shown in Fig. 3, in which the relief height along the center of a flagellum image is modulated with a period of 0.4 μm. The cell membrane of a flagellum is not rigid, and the flagellum can have a modulated shape (*14*). It is likely that the observed modulation reflects the flexibility of the cell membrane. In one AFM image, we observed a thin line of 0.1-μm width extending from the tip of a 0.25-μm width flagellum. This may be an image of internal microtubules (*14*) where the surrounding cell membrane was accidentally broken.

As described above the finest feature observed is 0.1 μm in width. Three factors limit resolution: (i) diffraction; (ii) x-ray dose; and (iii) exposure time. (i) Diffraction-limited resolution is given by $(g\lambda)^{1/2}$, where λ is the x-ray wavelength and g is the specimen to resist distance. The sperm head and most parts of the flagella are considered to have stuck to the resist surface, and the greatest g value was that of the head top, 1.7 μm. Therefore, the maximum diffraction blurring was 0.07 μm for λ = 3 nm, and the diffraction is not considered to have been the limiting factor in our experiment. (ii) In order to achieve the best resolution of ~0.02 μm in PMMA resist, an x-ray dose of 1 kJ/cm^3 is required (*15*). In our experiment the x-ray flux was 5 to 10 mJ/cm^2, which corresponds to an absorbed dose of 100 to 200 J/cm^3 in resist. A dose lower by a factor of 5 to 10 might degrade the resolution of PMMA to ~0.1 μm. Some roughness on the resist surface seen in Fig. 2B might be attributable to the low x-ray dose. (iii) Localized x-ray absorption due to the specimen inhomogeneities causes distortion of microstructures during the exposure. The maximum allowable exposure time has been calculated to be proportional to the resolution divided by the square root of the x-ray dose (*16*). For our 500-ps x-ray pulse, the resolution would be 0.06 μm (*17*). The 500-ps exposure time would not have been the limiting factor marginally. If the x-ray dose is to be increased for improving the resist resolution, the exposure time could limit the resolution. Although detailed experiments are required to verify the theory presented in (*16*), x-ray exposures longer than 1 ns would not be allowed for the resolution better than 0.1 μm.

REFERENCES AND NOTES

1. J. Kirz and D. Sayre, *X-ray Microscopy*, G. Schmahl and D. Rudolph, Eds. (Springer-Verlag, Berlin, 1984), pp. 262–267.
2. R. Feder *et al.*, *Science* **197**, 259 (1977); see also papers in D. Sayre, M. Howells, J. Kirz, H. Rarback, Eds., *X-ray Microscopy II* (Springer-Verlag, Berlin, 1988).
3. X-rays are absorbed locally because of specimen inhomogeneities. When the exposure time is long, the localized heat will be conducted away. However, exposure time should be short enough to avoid blurring caused by biological motions. Heat conduction becomes less effective for shorter exposures, in which case localized heat brings about expansion of the x-ray absorbing features. In order to record the original shape of the specimen, the exposure should be terminated before the expansion distorts the microstructures. For the detailed discussion, see J. C. Solem, *J. Opt. Soc. Am. B* **3**, 1551 (1986).
4. R. Feder *et al.*, *Science* **227**, 63 (1985).
5. P. C. Cheng, D. M. Shinozaki, K. H. Tan, in *X-ray Microscopy*, P. C. Cheng and G. C. Jan, Eds. (Springer-Verlag, Berlin, 1987), pp. 65–104.
6. G. Binning, C. F. Quate, Ch. Gerber, *Phys. Rev. Lett.* **56**, 930 (1986).
7. We measured the absolute conversion efficiency of the laser energy to x-rays in various kinds of targets. Angular distributions of x-ray and debris emissions were observed. The optimal target material, laser

power density, and angular position of the specimen were determined from this study. The most important finding in our study is that the water protects the recording x-ray resist from debris.

8. There are some reports of imaging hydrated specimens with laser pulses of several tens of joules of energy. To our knowledge, there was only one report of observing specimen in water with a laser plasma [R. W. Eason, M. Clague, R. Cherry, *Annual Report* (Rutherford Appleton Laboratory, Didcot, United Kingdom, 1985), p. A4.2.5] They used 30- to 40-J, 1-ns laser pulses. R. A. Cotton *et al.* (paper presented at the International Conference on X-Ray Microscopy, King's College, London, September 1990) reported that their x-ray flux produced by a 0.5-J, 25-ns laser pulse was sufficient for imaging dehydrated specimens but insufficient for hydrated specimens.
9. R. J. Rosser *et al.*, *Appl. Opt.* **26**, 4313 (1987).
10. The x-ray from our laser plasma showed a broad spectrum peaked at 2.8 nm. The water thickness in the experiment was estimated to be 3 μm from the transmission through the specimen. By taking account of the spectral dependence of the transmission through the 0.1-μm Si_3N_4 membrane and 3 μm of water and the sensitivity of the PMMA resist, the spectrum effective to the resist exposure was calculated. The main contribution comes from the x-rays of 2.4- to 3.0-nm wavelength. The contribution of x-rays outside the water-window region is negligibly small.
11. G. Giudice, Ed., *The Sea Urchin Embryo* (Springer-Verlag, Berlin, 1987), pp. 23–29.
12. When the dissolution rate R of a resist has a relation with the x-ray dose E of $R \propto E^n$, the relief height h is given by $h = (1 - T^n)d$, where T is the transmission of the specimen and d is the developed resist depth. The integrated density of the specimen can be calculated from the transmission and the absorption coefficient.
13. Living cells are mainly composed of proteins, lipids, and water. In proteins and lipids, the density of carbon is roughly 0.7 g/cm^3 from the data in (*16*). Nitrogen contained in protein contributes an additional 10% to the absorption.
14. A flagellum consists of the so-called axoneme and a ciliary membrane. The axoneme is made of nine outer microtubule doublets and two central microtubules. Outer doublets are arranged in a circle and connected to the center tubules by radial spokes. Periodicity of 0.2 to 0.4 μm is not known in this structure. R. D. Allen [*J. Cell. Biol.* **37**, 825 (1968)] reported EM images of transverse section through flagella of a unicellular organism *Tetrahymena*. In his pictures, the shape of the ciliary membrane is irregular and shows the flexibility of the ciliary membrane. Flagella of various species are considered to have the similar structure.
15. C. Jacobsen *et al.*, in *X-ray Microscopy II*, D. Sayre, M. Howells, J. Kirz, H. Rarback, Eds. (Springer-Verlag, Berlin, 1988), pp. 253–262.
16. R. A. London, M. D. Rosen, J. E. Trebes, *Appl. Opt.* **28**, 3397 (1989).
17. According to (*16*), the maximum allowable exposure time for 0.03-μm resolution is 27 ps when the x-ray dose is 15 kJ/g and the ratio of specific heats γ is 1.1. In our experiment, x-ray flux was 5 to 10 mJ/cm^2 and the x-ray dose in the sperm was 100 to 200 J/g. For the 500-ps duration x-ray exposure, the resolution is calculated to be ~0.06 μm.
18. The authors thank M. Morisawa of Misaki Marine Biological Station of the Tokyo University for providing the sea urchin, and Seiko Instruments, Inc., for the measurement by AFM.

19 November 1990; accepted 6 February 1991

Atmospheric Lifetime of CHF_2Br, a Proposed Substitute for Halons

R. TALUKDAR, A. MELLOUKI, T. GIERCZAK,* J. B. BURKHOLDER, S. A. MCKEEN, A. R. RAVISHANKARA†

The rate coefficients, k_1, for the reaction of OH with CHF_2Br have been measured using pulsed photolysis and discharge flow techniques at temperatures (T) between 233 and 432 K to be $k_1 = (7.4 \pm 1.6) \times 10^{-13} \exp[-(1300 \pm 100)/T]$ cubic centimeters per molecule per second. The ultraviolet absorption cross sections, σ, of this molecule between 190 and 280 nanometers were measured at 296 K. The k_1 and σ values were used in a one-dimensional model to obtain an atmospheric lifetime of approximately 7 years for CHF_2Br. This lifetime is shorter by approximately factors of 10 and 2 than those for CF_3Br and CF_2ClBr, respectively. The ozone depletion potentials of the three compounds will reflect these lifetimes.

SINCE THE SIGNING OF THE MONTREAL protocol (*1*) curtailing, and eventually banning, the production of chemicals that can destroy stratospheric ozone, many new compounds have been proposed as substitutes for the regulated compounds. Bromocarbons (Halons), for example, CF_3Br, and CF_2ClBr, which are used as fire-extinguishing agents, are major anthropogenic sources of stratospheric Br and will have to be replaced (*1*). One proposed substitute, CHF_2Br (*2*), has good fire-suppression characteristics (*3*). This molecule, because of the presence of an H atom, reacts with OH free radicals in the troposphere; as a result, the quantity of this molecule transported to the stratosphere is reduced. To judge the acceptability of this replacement, it is necessary to know the fraction of CHF_2Br released at the earth's surface that will reach the stratosphere. A measure of this quantity is the tropospheric lifetime of the compound. Two processes that can destroy this molecule in the troposphere and thus reduce its transport to the stratosphere are (i) the reaction with the OH free radical

$$OH + CHF_2Br \rightarrow CF_2Br + H_2O; k_1 \quad (1)$$

and (ii) photolysis. The latter process is quantified by measurement of the absorption cross section, σ, in the ultraviolet (UV) region. We have measured the rates of these two processes and calculated the tropospheric lifetime.

We measured the rate coefficient, k_1, using two complimentary techniques: (i) discharge flow with laser magnetic resonance detection (DF-LMR) of OH and (ii) pulsed laser photolysis with laser-induced fluorescence detection (PP-LIF) of OH [see (*4, 5*)]. The experimental conditions used to measure k_1 are listed in Table 1. In the pulsed photolysis experiments, HONO was used as the OH precursor. Because CHF_2Br is nearly transparent at 355 nm ($\sigma < 10^{-24}$ cm^2), the wavelength at which HONO was photolyzed, secondary reactions of CHF_2Br photofragments were minimized. The mass flow rates of all compounds flowing through the reactor were measured with calibrated mass flowmeters, and the flow rates were then used to determine the concentration of CHF_2Br. The sample of CHF_2Br had an analyzed purity of 98.8%; CF_2ClBr (1%) and CF_2HCl (0.2%) were the main impurities. We also analyzed the sample for the possible presence of Br_2 and HBr, which react very rapidly with OH, using UV and infrared (IR) spectral measurements and found them to be less than 1 ppm by volume each.

Secondary reactions of OH were negligible, as reported in earlier papers dealing with the OH reaction rate coefficient measurements (*4, 5*), under our experimental conditions (see Table 1). There was good agreement between data obtained by two independent methods. We are confident that our measurements do not have any large systematic errors. In the DF-LMR study, we could not measure k_1 below 268 K because CHF_2Br sticks on the walls of the reactor.

The measured values of k_1 (Table 1 and Fig. 1) can be expressed in the Arrhenius form as

$$k_1 = (7.4 \pm 1.6) \times 10^{-13} \exp[-(1300 \pm 100)/T] \text{ cm}^3 \text{ molecule}^{-1} \text{ s}^{-1} \quad (2)$$

for temperatures (T) between 233 and 352 K. Even though k_1 was measured up to 432 K, data at $T > 352$ K are not included in the fit because of the slight curvature in the Arrhenius plot at the higher temperatures and because we use measurements made at

National Oceanic and Atmospheric Administration (NOAA), Aeronomy Laboratory, R/E/AL2, 325 Broadway, Boulder, CO 80303, and The Cooperative Institute for Research in Environmental Sciences, University of Colorado, Boulder, CO 80309.

*On leave from the Department of Chemistry, Warsaw University, Zwirki i Wigury 101, 02-089 Warsaw, Poland.
†To whom correspondence should be addressed at NOAA. Also affiliated with the Department of Chemistry and Biochemistry, University of Colorado, Boulder, CO 80309.